

Azimuthal anisotropy in a jet absorption model with fluctuating initial geometry in heavy ion collisions

Jiangyong Jia^{1,2}

¹*Department of Chemistry, Stony Brook University, Stony Brook, NY 11794, USA*

²*Physics Department, Brookhaven National Laboratory, Upton, NY 11796, USA*

(Dated: November 20, 2018)

The azimuthal anisotropy due to path-length dependent jet energy loss is studied in a simple jet absorption model that include event by event fluctuating Glauber geometry. Significant anisotropy coefficients v_n are observed for $n = 1, 2$ and 3 , but they are very small for $n > 3$. These coefficients are expected to result in a “ridge” for correlations between two independently produced jets. The correlations between the orientation of the n^{th} -order anisotropy induced by jet absorption (Φ_n^{QP}) and the n^{th} -order participant plane (Φ_n^{PP}) responsible for harmonic flow are studied. Tight correlations are observed for $n = 2$ in mid-central collisions, but they weaken significantly for $n \neq 2$. The correlations are positive for $n \leq 3$, but become negative in central collisions for $n > 3$. The dispersion between Φ_n^{QP} and Φ_n^{PP} is expect to break the factorization of the Fourier coefficients from two-particle correlation $v_{n,n}$ into the single particle v_n , and has important implications for the high- p_T ridge phenomena.

PACS numbers: 25.75.Dw

I. INTRODUCTION

Recently, a lot of attentions are focused on the study of the azimuthal anisotropy of the particle production in heavy ion collisions at the Relativistic Heavy Ion Collider (RHIC) and the Large Hadron Collider (LHC). This anisotropy is usually expanded into a Fourier series:

$$\frac{dN}{d\phi} \propto 1 + 2 \sum_{n=1}^{\infty} v_n \cos n(\phi - \Phi_n) \quad (1)$$

with v_n and Φ_n represent the magnitude and direction of n^{th} -order anisotropy, respectively. At low p_T , v_n is driven by the anisotropic pressure gradient associated with the initial spatial asymmetries, with more particles emitted in the direction of largest gradients [1]. Asymmetries giving rise to non-zero v_n are associated with either average shape (for $n = 2$) or shapes arising from spatial fluctuations of the participating nucleons [2–5]. They can be characterized by a set of multi-pole components (also known as “eccentricities”) at different angular scale, calculated from the participating nucleons at (r, ϕ) [3]:

$$\epsilon_n = \frac{\sqrt{\langle r^2 \cos n\phi \rangle^2 + \langle r^2 \sin n\phi \rangle^2}}{\langle r^2 \rangle}. \quad (2)$$

The orientations of the minor axis for each moment n , also known as the participant plane (PP) are given by

$$\Phi_n^{\text{PP}} = \frac{\text{atan2}(\langle r^2 \sin n\phi \rangle, \langle r^2 \cos n\phi \rangle)}{n} + \frac{\pi}{n} \quad (3)$$

When fluctuations are small and linearized hydrodynamics is applicable, each moment of the flow v_n is expected to be independently driven by ϵ_n along $\Phi_n^{\text{PP}} = \Phi_n$ [3]. This may not be true when the fluctuations are large, as the non-linear effects may lead to significant mixing between harmonic flow of different order [6]. In this paper,

they are assumed to be the same to facilitate the study of the correlations between Φ_n of different physics origins.

At high p_T ($p_T \gtrsim 10$) GeV, the v_n is understood to be driven by the path-length dependent energy loss of jets traversing the medium, with more particles emitted along the direction of shortest path-length (or direction of smallest jet attenuation) [7, 8]. In contrast to flow which is sensitive to the global geometry manifested through the global evolution of the created matter, this anisotropy is more sensitive to the local density experienced by the jets as they traverse the matter. Nevertheless, since both flow and jet quenching are influenced by the same geometry, the directions of largest pressure gradient for flow and direction of smallest jet attenuation are strongly correlated. In fact, they are often implicitly assumed to be the same in many theoretical calculations [9–14]. An explicit study of the correlation between the two directions can help clarifying this assumption.

In this paper, we estimate the high- p_T anisotropy coefficients v_n and their associated directions Ψ_n^{QP} (QP stands for “quenching plane”) using a simple jet absorption model with event by event fluctuating Glauber geometry. We study the correlations between Ψ_n^{PP} and Ψ_n^{QP} , and discuss implications of these correlations for the interpretation of the “ridge” phenomena in two-particle correlations (2PC).

II. MODEL

We use a simple jet absorption/Glauber model of Ref. [15] to calculate v_n and Ψ_n^{QP} . This model has been used previously to study the centrality and path-length dependence of single particle suppression R_{AA} , dihadron suppression I_{AA} and v_2 . Back-to-back jet pairs are generated according to the binary collision density profile (ρ_c) in the transverse (xy) plane with random orienta-

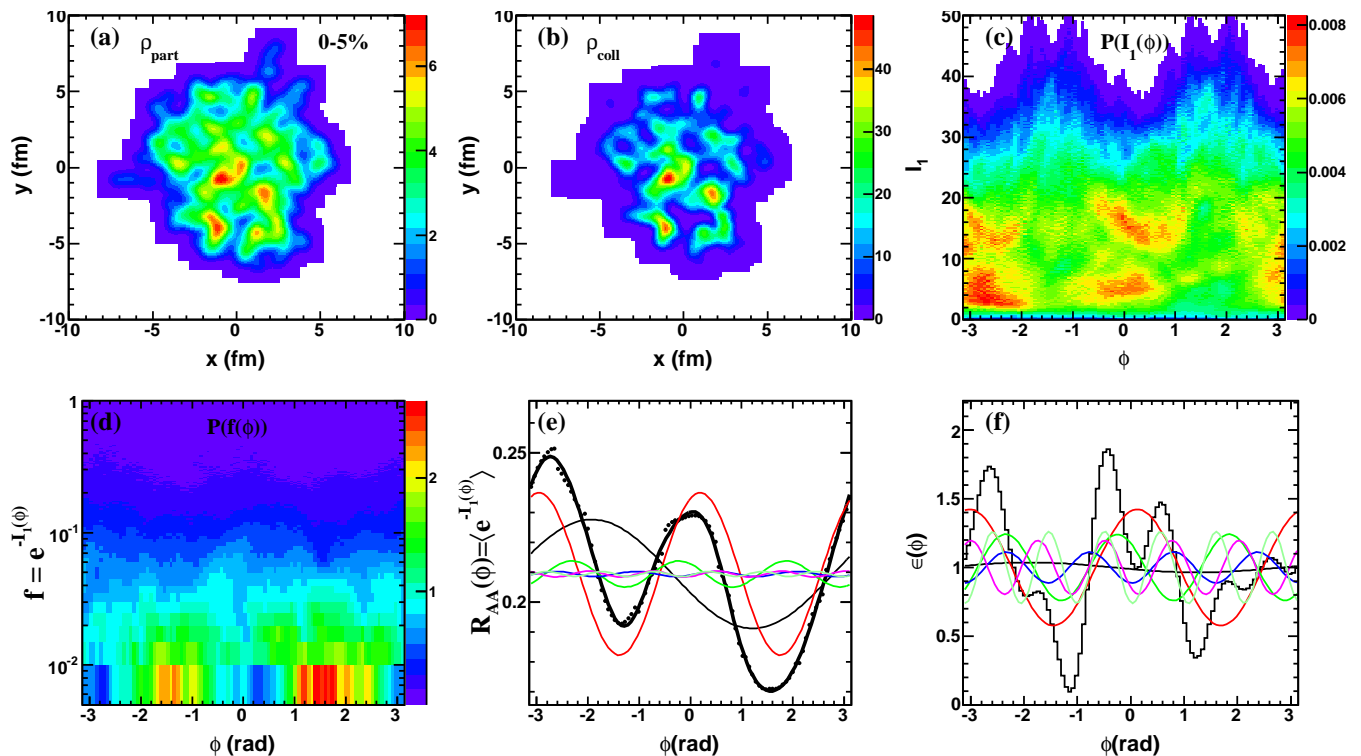


FIG. 1: (Color online) The complete set of output obtained in the jet absorption model for one event in 0-5% centrality interval: (a) the participant density profile (ρ_p); (b) the collision density profile (ρ_c), (c) the probability distribution of the path-length integral I_1 , (d) the probability distribution of jet surviving the exponential attenuation, (e) the distribution of survival rate as function of azimuth angle, (f) the initial spatial asymmetry of the participants calculated via Eq. 7. The original impact parameter of the event is aligned along the x -axis.

71 tion. They are then propagated through the medium, 72 whose density is given by the participant density profile 73 (ρ_p). Both profiles are generated with a Monte Carlo 74 Glauber model with event by event fluctuation of po- 75 sitions of nucleons in Au ions [16]. The nucleons are 76 sampled from a Woods-Saxon distribution with a radius 77 of 6.38 fm and diffuseness of 0.535 fm, with a nucleon- 78 nucleon cross-section of $\sigma_{nn} = 42$ mb. In order to have 79 smooth distributions for ρ_c and ρ_p , the nucleons are as- 80 sumed to have a Gaussian profile in transverse plane with 81 a width of $r_0 = 0.4$ fm in x and y direction similar to 82 Ref [10]. The value of r_0 is varied from 0.2-0.4 fm, and 83 the nucleon is also assumed to be a uniform disk with a 84 radius of $\sqrt{\sigma_{nn}/\pi}/2 = 0.58$ fm. However the final results 85 are found to be insensitive to the details of the nucleon 86 shape, except in peripheral collisions.

87 The jet quenching is implemented via exponential at- 88 tenuation $f = e^{-\kappa I}$, where the matter integral I is cal- 89 culated as

$$I_m = \int_0^\infty dl \frac{l^m}{l+l_0} \rho(\vec{\mathbf{r}} + (l+l_0)\hat{\mathbf{v}}) \quad (4)$$

$$\approx \int_0^\infty dl l^{m-1} \rho(\vec{\mathbf{r}} + l\hat{\mathbf{v}}), \quad m = 1, 2. \quad (5)$$

90 for jet generated at $\vec{\mathbf{r}} = (x, y)$ and propagated along

91 direction $\hat{\mathbf{v}}$. They corresponds to l^{m+1} dependence of 92 absorption ($\propto l^m dl$) in a longitudinal expanding or 1+1D 93 medium ($\propto 1/(l_0+l)$) with a thermalization time of $l_0 =$ 94 $c\tau_0$. The l_0 is fixed to 0 by default, but we have checked 95 the v_n do not change much for $l_0 < 0.3$ fm [10]. The 96 two cases, $m = 1$ and $m = 2$, are motivated for the l 97 dependence expected for radiative and AdS/CFT energy 98 loss in 1+1D medium [17, 18], respectively.

99 The absorption coefficient κ controls the jet quenching 100 strength and is the only parameter in this calculation. 101 It is tuned to reproduce $R_{AA} = \langle e^{-\kappa I_m} \rangle \sim 0.19$ for 0- 102 5% π^0 data at RHIC after averaging over many Glauber 103 events [19]. This leads to a value of $\kappa = 0.1473$ fm $^{-1}$ and 104 0.0968 fm $^{-2}$ for $m = 1$ and 2, respectively.

105 III. RESULTS

106 Figure 1 summarize the basic information obtained 107 from this procedure for one typical Au-Au event in 0-5% 108 centrality interval. Panels (a) and (b) shows the den- 109 sity profile for ρ_p and ρ_c , respectively. Panel (c) shows 110 the normalized probability distribution of I_1 : $P(I_1(\phi))$, 111 which is obtained by calculating I_1 over all possible di- 112 jet production point ρ_c and jet propagation direction ϕ .

113 This distribution exhibit characteristic high density and
 114 low density regions in (I_1, ϕ) space, presumably reflect-
 115 ing spatial correlation between the ρ_c and ρ_p profiles.
 116 Panel (d) shows the normalized probability distribution
 117 of the attenuation $e^{-\kappa I_1}$. Panel (e) shows the $\langle e^{-\kappa I_1} \rangle$ av-
 118 eraged along the y-axis in Panel (d) as a function ϕ , which
 119 is precisely the azimuthal angle dependent suppression
 120 $R_{AA}(\phi)$. A clear anti-correlation can be seen between
 121 the peak magnitude of the $R_{AA}(\phi)$ and breadth of the
 122 I_1 distribution in Panel (c). This distribution can also
 123 be obtained by randomly generating many di-jet pairs
 124 according the ρ_c and propagating them through ρ_p via
 125 Eq. 6. We expand it into a Fourier series:

$$R_{AA}(\phi) = R_{AA}^0 \left(1 + 2 \sum_{n=1}^{\infty} v_n^{\text{QP}} \cos n(\phi - \Phi_n^{\text{QP}}) \right), \quad (6)$$

126 where R_{AA}^0 represents the average suppression, v_n^{QP} and
 127 Φ_n^{QP} represent the magnitude and direction of n^{th} -order
 128 harmonic of emission probability distribution, respec-
 129 tively. Similar studies of $R_{AA}(\phi)$ were pursued before
 130 in Ref. [12] for a pQCD energy loss in a event by event
 131 hydrodynamic underlying event. However it focused pri-
 132 marily on the influence of fluctuations on the event-
 133 averaged $R_{AA}(\phi)$ distribution relative to the 2nd-order
 134 event plane (EP).

135 Figure 1 (f) shows a distribution calculated from ϵ_n
 136 and Φ_n^{QP} :

$$\epsilon(\phi) = 1 + 2 \sum_{n=1}^{\infty} \epsilon_n \cos n(\phi - \Phi_n^{\text{PP}}). \quad (7)$$

137 It visualizes the shape of the initial geometry that is
 138 transformed into the final momentum anisotropy via ei-
 139 ther flow or jet quenching. A good alignment is seen
 140 between Φ_n^{PP} and Φ_n^{QP} for $n \leq 3$. It also shows that the
 141 large ϵ_n for $n > 3$ are strongly damped after jet absorp-
 142 tion, leading to very small values of v_n^{QP} for $n > 3$.

143 The study shown in Fig. 1 can be repeated for many
 144 events. We divide the simulation data into 5% centrality
 145 intervals, each containing about 2500 events. Figure 2
 146 shows the distribution of $\Phi_n^{\text{PP}} - \Phi_n^{\text{QP}}$ for two centrality
 147 intervals. Strong positive correlations are obtained for
 148 $n = 1, 2$ and 3, while the correlations are rather weak or
 149 even become negative for $n > 3$ ¹.

150 In heavy ion collisions at RHIC and LHC, the v_n is
 151 usually measured from particle distribution relative to
 152 Ψ_n via Eq. 1 [20]. However it has also been derived from
 153 the Fourier coefficients of two-particle correlation in rel-
 154 ative azimuthal angle $\Delta\phi = \phi^a - \phi^b$ [21]:

$$\frac{dN_{\text{pairs}}}{d\Delta\phi} \propto 1 + 2 \sum_{n=1}^{\infty} v_{n,n}(p_{\text{T}}^a, p_{\text{T}}^b) \cos n\Delta\phi, \quad (8)$$

155 with

$$v_{n,n}(p_{\text{T}}^a, p_{\text{T}}^b) = v_n(p_{\text{T}}^a) v_n(p_{\text{T}}^b). \quad (9)$$

¹ Φ_n^{PP} in Eq. is calculated with r^2 weighting. We have also re-
 peated the study using r^n weighting for $n > 1$ and r^3 weighing
 for $n = 1$ [5], but very little differences are seen.

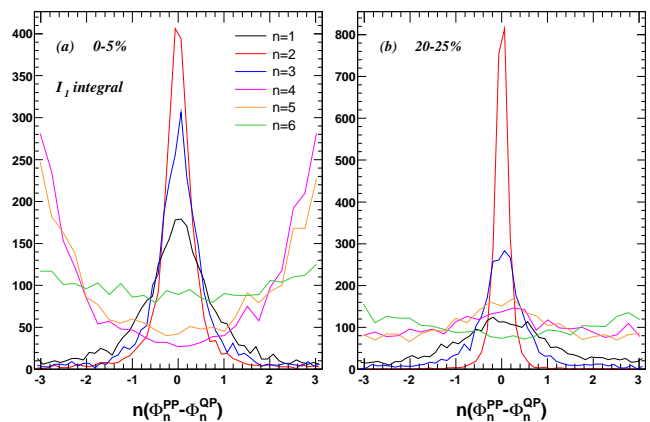


FIG. 2: (Color online) The correlation between participant plane Φ_n^{PP} and quenching plane Φ_n^{QP} for $n = 1 - 6$ calculated for I_1 path-length dependence and for (a) 0-5% and (b) 20-25% centrality interval.

156 The fact that the quenching plane and participant plane
 157 do not align exactly with each other implies that the
 158 v_n measured relative to Ψ_n^{PP} is not the same as those
 159 contributing to the 2PC in Eq. 8. In other words, it is
 160 possible that the v_n obtained from single particle analysis
 161 is only a fraction of the true anisotropy resulting from jet
 162 quenching:

$$v_n = v_n^{\text{QP}} \langle \cos n(\Phi_n^{\text{PP}} - \Phi_n^{\text{QP}}) \rangle \quad (10)$$

163 Since what is measured in experiment is the event plane
 164 not the PP, it is important to check whether the event
 165 plane align with QP or not, for example in a hydrody-
 166 namic model calculation.

167 Figure 3 (a) and (c) summarize the centrality depen-
 168 dence of v_n^{QP} for $n = 1-6$ and for I_1 and I_2 , respec-
 169 tively. Significant v_n^{QP} signals are observed for $n \leq 3$,
 170 while higher-order v_n^{QP} are usually smaller than 1%. The
 171 v_2^{QP} and $v_4^{\text{QP}} - v_6^{\text{QP}}$ all show strong centrality dependence,
 172 while the v_1^{QP} and v_3^{QP} show little centrality dependence
 173 for $N_{\text{part}} > 100$. Interestingly, the value of the v_1^{QP} is
 174 consistently larger than that for v_3^{QP} , and it even ex-
 175 ceeds v_2^{QP} value in most central collisions. This behavior
 176 suggest that the path-length dependence of energy loss
 177 and initial dipole asymmetry from fluctuations corroborate
 178 to produce a large v_1^{QP} . This large v_1^{QP} is expect
 179 to contribute to the high- p_{T} v_1 signal observed by the
 180 ATLAS Collaboration [21]. Figure 3 also shows that the
 181 I_2 type of path-length dependence induces significantly
 182 larger v_n^{QP} than that for I_1 : the increase is almost a fac-
 183 tor of two for $n = 1$ and $n = 3$. This is also observed in
 184 other studies before [10, 18].

185 Figure 3 (b) and (d) summarize the centrality depen-
 186 dence of $\langle \cos n(\Phi_n^{\text{PP}} - \Phi_n^{\text{QP}}) \rangle$ for $n = 1 - 6$ and for I_1
 187 and I_2 , respectively. As indicated by Eq. 10, this repre-
 188 sents the reduction factor of the v_n when it is measured
 189 relative to the Φ_n^{PP} . The reduction is small for $n = 2$,
 190 except in central collisions where it reaches 15% for I_1

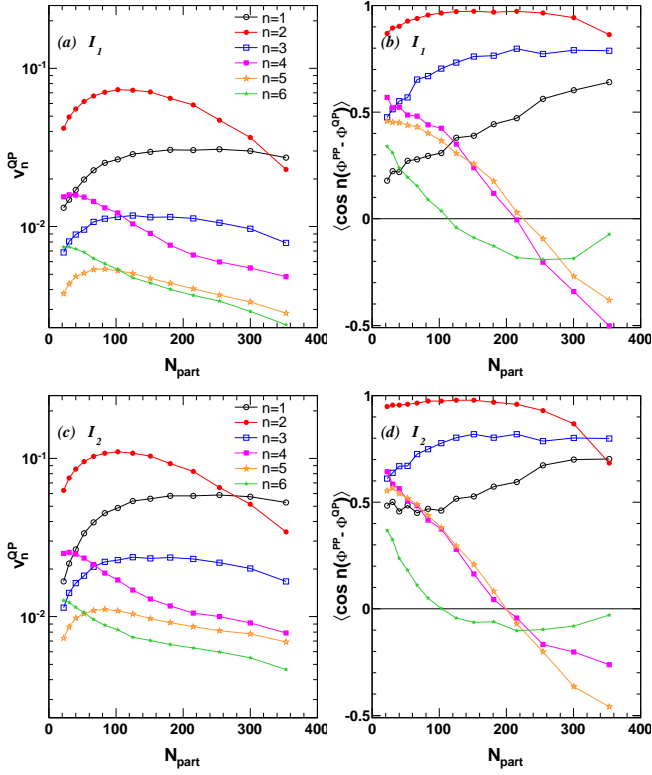


FIG. 3: (Color online) The centrality dependence of anisotropy coefficients v_n^{QP} (left panels) and correlation between the participant plane and quenching plane $\langle \cos n(\Phi_n^{PP} - \Phi_n^{QP}) \rangle$ (right panels) for I_1 type of path-length dependence (top panels) and I_2 types of path-length dependence (bottom panels). Note that the values of v_n^{QP} are positive by construction according to Eq. 6.

191 and 30% for I_2 . However the reduction is significantly
 192 larger for $n = 1$ and 3, reaching about 50% for $n = 1$ in
 193 mid-central collisions. The $\langle \cos n(\Phi_n^{PP} - \Phi_n^{QP}) \rangle$ value
 194 becomes negative for $n > 3$ in central collisions, reflecting
 195 an anti-correlation between Φ_n^{PP} and Φ_n^{QP} (already shown
 196 in Fig. 2). Interestingly, $\langle \cos n(\Phi_n^{PP} - \Phi_n^{QP}) \rangle$ values for
 197 $n = 1$ are always smaller than that for $n = 3$ (more
 198 misalignment), while v_1^{QP} is always larger than v_3^{QP} .

199 The dispersion between the Φ_n^{QP} and Φ_n^{PP} has impor-
 200 tant implications on the factorization relation Eq. 9. The
 201 factorization of $v_{n,n}$ into v_n is obviously valid for cor-
 202 relations between two low p_T particles (soft-soft correla-
 203 tion) as both are modulated around Φ_n^{PP} . The fac-
 204 torization should also be valid for correlation between
 205 a low- p_T particle and a high- p_T particle (soft-hard cor-
 206 relation) since it involves the projection of the v_n onto
 207 Φ_n^{PP} , i.e. $v_{n,n}(p_T^a, p_T^b) = v_n(p_T^a)v_n^{QP}(p_T^b)\langle \cos n(\Phi_n^{PP} -$
 208 $\Phi_n^{QP}) \rangle = v_n(p_T^a)v_n(p_T^b)$. Experimental data indeed sup-
 209 port this [21, 23]. However the correlation between two
 210 high- p_T particles from two independent hard-scattering
 211 processes (hard-hard correlation) is expected to be larger
 212 than the product of the two single particle v_n :

$$v_{n,n}(p_T^a, p_T^b) = v_n^{QP}(p_T^a)v_n^{QP}(p_T^b) \quad (11)$$

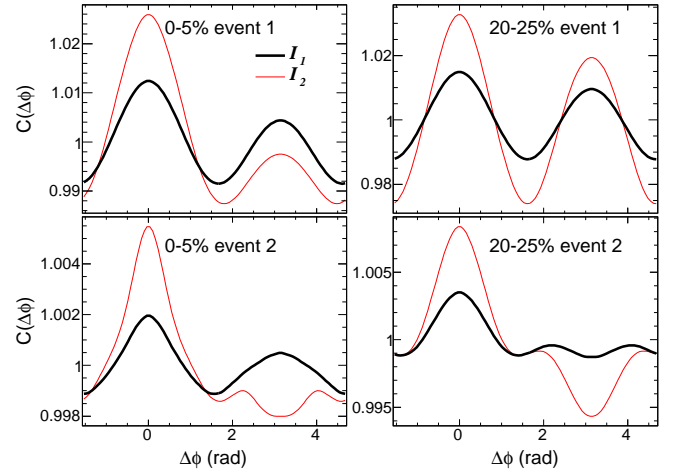


FIG. 4: (Color online) The expected long-range structures for correlations between two high p_T particles from independent hard-scattering processes. They are shown for two typical events in 0-5% centrality interval (left panels) and 20-25% centrality interval (right panels); each of them should be regarded as the distributions obtained for many events with identical initial geometry.

$$= \frac{v_n(p_T^a)v_n(p_T^b)}{\langle \cos n(\Phi_n^{PP} - \Phi_n^{QP}) \rangle^2}.$$

213 Therefore, the factorization can not work simultaneously
 214 for soft-soft, soft-hard and hard-hard correlations.

215 The large anisotropy coefficients v_n^{QP} also has im-
 216 portant consequences for the “ridge” observed in two-
 217 particle correlations [21–23]. This “ridge” is understood
 218 to be the result of the constructive contribution of har-
 219 monics at $\Delta\phi \sim 0$. In the literature, it is referred to
 220 as either the “soft-ridge” [24, 25] for soft-soft correlation
 221 or “hard-ridge” [22, 26] for soft-hard correlation, respec-
 222 tively. Here we show that the correlation between two
 223 independently produced high- p_T jets can also produce
 224 the “ridge”-like structure. This “hard-hard ridge” can be
 225 calculated on a probability basis event-by-event by sim-
 226 ply self-convoluting the $R_{AA}(\phi)$ distribution like Fig. 1
 227 (e). Examples of these structures are shown in Fig. 4
 228 for two representative events in both 0-5% and 20-25%
 229 centrality intervals. The magnitude of the ridge, as well
 230 as the away-side shape changes dramatically from event
 231 to event. They also changes a lot between the I_1 and I_2
 232 types of path-length dependence jet absorption.

233 Figure 5 show the long-range structures (solid lines)
 234 obtained from the jet absorption model, averaged over
 235 many events. The ridge magnitude increases with cen-
 236 trality to about 1.5% (4%) for I_1 (I_2) path-length de-
 237 pendence in mid-central collisions. This signal should be
 238 measurable with the large statistics dataset from LHC.
 239 The dashed lines in Fig. 5 show the 2PC predicted from
 240 the v_n measured relative to Φ_n^{PP} . Clearly the misalign-
 241 ments between Φ_n^{QP} and Φ_n^{PP} reduces the ridge mag-
 242 nitude. The reduction is almost 50% in most central col-
 243 lisions, but decrease to about 20% in mid-central collisions.

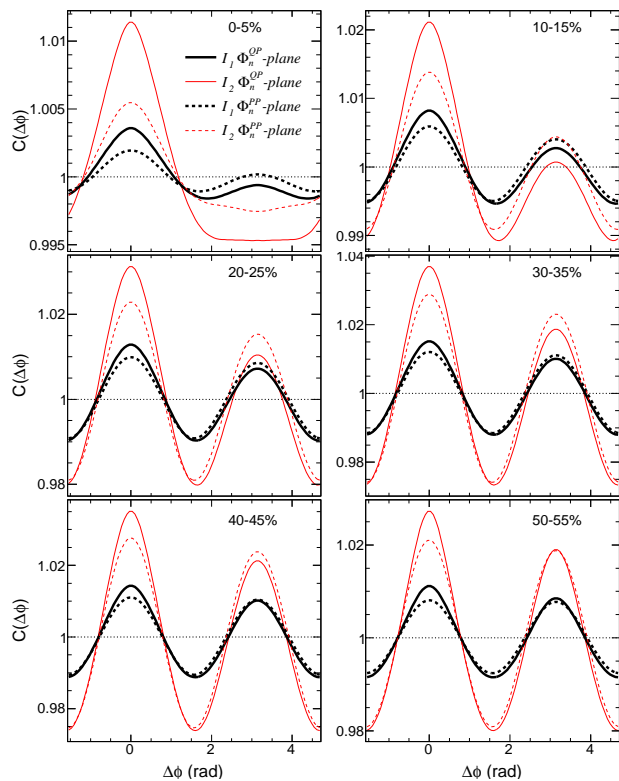


FIG. 5: (Color online) The expected long-range structures for correlations between two high p_T particles from two independent hard-scattering processes (solid lines) and those calculated from single particle v_n^{QP} relative to participant planes (dashed lines) for various centrality intervals. They are average distribution over many events for a given centrality intervals. The thick (thin) lines denote the I_1 (I_2) type of path-length dependence.

This suggests the difference between the measured ridge and those predicted by the event plane method could be

large and measurable.

IV. CONCLUSION

The anisotropy of high- p_T particle is studied in a simple jet absorption framework with event by event fluctuating geometry. The harmonic coefficients v_n are found to be significant for $n = 1 - 3$ ($> 1\%$) but become very small for $n > 3$. The correlation between the quenching plane and participant plane are studied. A strong de-correlation is found for $n = 2$ in central collisions and for $n = 1$ and 3 over the full centrality range. The correlations become negative for $n > 3$ in central collisions. This de-correlation, if also confirmed between the event plane and the quenching plane (e.g via hydrodynamic model that has dijets embedded), is expected to break the global factorization of the two particle Fourier coefficient $v_{n,n}$ into the v_n for the two single particles. It would also imply that the high- p_T v_n measured relative to the event plane could be significantly smaller than the true anisotropy from path-length dependent jet energy loss. These jet quenching v_n also give rise to long range “ridge” structure in two-particle correlations. The predicted ridge amplitude is on the order of 0.5-4% depending on the centrality and functional form of the l dependence of the energy loss, and should be measurable at the LHC using the correlations between two high- p_T particles with a large rapidity separation. Our study bear some similarities to Ref. [14]. However, Ref. [14] uses a cumulant expansion framework instead of Monte Carlo Glauber model for initial geometry, and that it focus on the soft-hard ridge instead of the hard-hard ridge in our case.

Discussions with Jinfeng Liao is acknowledged. This research is supported by NSF under award number PHY-1019387.

-
- [1] J. Y. Ollitrault, Phys. Rev. D **46**, 229 (1992).
 [2] B. Alver and G. Roland, Phys. Rev. C **81**, 054905 (2010) [Erratum-ibid. C **82**, 039903 (2010)].
 [3] B. H. Alver, C. Gombeaud, M. Luzum and J. -Y. Ollitrault, Phys. Rev. C **82**, 034913 (2010).
 [4] P. Staig and E. Shuryak, Phys. Rev. C **84**, 034908 (2011).
 [5] D. Teaney and L. Yan, Phys. Rev. C **83**, 064904 (2011).
 [6] Z. Qiu and U. W. Heinz, Phys. Rev. C **84**, 024911 (2011).
 [7] M. Gyulassy, I. Vitev and X. N. Wang, Phys. Rev. Lett. **86**, 2537 (2001).
 [8] A. Adare *et al.* [PHENIX Collaboration], Phys. Rev. Lett. **105**, 142301 (2010).
 [9] S. A. Bass, C. Gale, A. Majumder, C. Nonaka, G. -Y. Qin, T. Renk and J. Ruppert, Phys. Rev. C **79**, 024901 (2009).
 [10] J. Jia and R. Wei, Phys. Rev. C **82**, 024902 (2010).
 [11] J. Jia, W. A. Horowitz and J. Liao, Phys. Rev. C **84**, 034904 (2011).
 [12] T. Renk, H. Holopainen, J. Auvinen and K. J. Eskola, arXiv:1105.2647 [hep-ph].
 [13] B. Betz, M. Gyulassy and G. Torrieri, Phys. Rev. C **84**, 024913 (2011).
 [14] X. Zhang and J. Liao, arXiv:1202.1047 [nucl-th], J. Liao and E. Shuryak, Phys. Rev. Lett. **102**, 202302 (2009).
 [15] A. Drees, H. Feng and J. Jia, Phys. Rev. C **71**, 034909 (2005).
 [16] B. Alver, M. Baker, C. Loizides and P. Steinberg, “The PHOBOS Glauber Monte Carlo,” arXiv:0805.4411 [nucl-ex].
 [17] P. M. Chesler, K. Jensen, A. Karch and L. G. Yaffe, Phys. Rev. D **79**, 125015 (2009).
 [18] C. Marquet and T. Renk, Phys. Lett. B **685**, 270 (2010).
 [19] A. Adare *et al.*, Phys. Rev. Lett. **101**, 232301 (2008).
 [20] A. M. Poskanzer and S. A. Voloshin, Phys. Rev. C **58**, 1671 (1998).
 [21] ATLAS Collaboration, arXiv:1203.3087 [hep-ex].

- ³¹⁶ [22] STAR Collaboration, Phys. Rev. C **80**, 064912 (2009). ³²¹ **79**, 051902 (2009) [arXiv:0806.4718 [nucl-th]].
- ³¹⁷ [23] CMS Collaboration, arXiv:1201.3158 [nucl-ex]. ³²² [26] G. Moschelli and S. Gavin, Nucl. Phys. A **830**, 623C
- ³¹⁸ [24] M. Daugherty [STAR Collaboration], J. Phys. G **35**, ³²³ (2009) [arXiv:0907.4362 [nucl-th]].
- ³¹⁹ 104090 (2008).
- ³²⁰ [25] S. Gavin, L. McLerran and G. Moschelli, Phys. Rev. C